Nanosecond Laser Treatment for Age-Related Macular Degeneration Does Not Induce Focal Vision Loss or New Vessel Growth in the Retina

Kirstan A. Vessey,[1] Tracy Ho,[1] Andrew I. Jobling,[1] Samuel A. Mills,[1] Mai X. Tran,[1] Alice Brandli,[1] Jackson Lam,[1] Robyn H. Guymer,[2] and Erica L. Fletcher[1]

[1]Department of Anatomy and Neuroscience, The University of Melbourne, Melbourne, Victoria, Australia
[2]Centre for Eye Research Australia, Royal Victorian Eye and Ear Hospital; Department of Surgery (Ophthalmology), The University of Melbourne, Victoria, Australia

Correspondence: Erica L. Fletcher, Department of Anatomy and Neuroscience, The University of Melbourne, Medical Building, Level 7, East Corner of Grattan Street and Royal Parade, Melbourne, Victoria 3010, Australia; elf@unimelb.edu.au.

KAV and TH contributed equally to the work presented here and should therefore be regarded as equivalent authors.

Submitted: October 5, 2017
Accepted: January 2, 2018

Citation: Vessey KA, Ho T, Jobling AI, et al. Nanosecond laser treatment for age-related macular degeneration does not induce focal vision loss or new vessel growth in the retina. *Invest Ophthalmol Vis Sci*. 2018;59:731–745. https://doi.org/10.1167/iovs.17-23098

Purpose. Subthreshold, nanosecond pulsed laser treatment shows promise as a treatment for age-related macular degeneration (AMD); however, the safety profile needs to be robustly examined. The aim of this study was to investigate the effects of laser treatment in humans and mice.

Methods. Patients with AMD were treated with nanosecond pulsed laser at subthreshold (no visible retinal effect) energy doses (0.15–0.45 mJ) and retinal sensitivity was assessed with microperimetry. Adult C57BL6J mice were treated at subthreshold (0.065 mJ) and suprathreshold (photoreceptor loss, 0.5 mJ) energy settings. The retinal and vascular responses were analyzed by fundus imaging, histologic assessment, and quantitative PCR.

Results. Microperimetry analysis showed laser treatment had no effect on retinal sensitivity under treated areas in patients 6 months to 7 years after treatment. In mice, subthreshold laser treatment induced RPE loss at 5 hours, and by 7 days the RPE had retiled. Fundus imaging showed reduced RPE pigmentation but no change in retinal thickness up to 3 months. Electron microscopy revealed changes in melanosomes in the RPE, but Bruch's membrane was intact across the laser regions. Histologic analysis showed normal vasculature and no neovascularization. Suprathreshold laser treatment did not induce changes in angiogenic genes associated with neovascularization. Instead pigment epithelium–derived factor, an antiangiogenic factor, was upregulated.

Conclusions. In humans, low-energy, nanosecond pulsed laser treatment is not damaging to local retinal sensitivity. In mice, treatment does not damage Bruch's membrane or induce neovascularization, highlighting a reduced side effect profile of this nanosecond laser when used in a subthreshold manner.

Keywords: retina, nanosecond laser, retinal rejuvenation therapy (2RT), retinal pigmented epithelium (RPE), choroid, vasculature, angiogenesis, mouse, human

Age-related macular degeneration (AMD) is the leading cause of irreversible severe vision loss in the elderly Western populations.[1,2] It is a multifactorial disease that involves a complex interplay between environmental (e.g., diet, smoking), demographic (e.g., age, sex, race), and genetic risk factors.[1,2] In the early stages of disease, there are common characteristic pathologies; specifically, thickening of Bruch's membrane, a five-layered semipermeable structure delineated by the choriocapillaris vasculature and the retinal pigment epithelium (RPE),[3–5] and the deposition of extracellular deposits called drusen between the RPE and Bruch's membrane.[6,7] Visual impairment seen in patients with AMD is a result of progressive damage to the photoreceptors, Bruch's membrane, the RPE, and the choroid at the macula, the central retina responsible for high-acuity vision. There are two forms of advanced AMD. Geographic atrophy, is characterized by gradual RPE atrophy and loss of the underlying photoreceptors, whereas neovascular AMD is characterized by the aberrant growth of vessels into the retina, usually from the choroid, termed "choroidal neovascularization" (CNV).[1,2]

In the past decade, several novel therapeutic agents that target the angiogenic factor known as vascular endothelial growth factor (VEGF) have been developed to slow blood vessel growth and have been found to be effective drugs for the treatment of CNV.[8,9] However, there are currently no effective therapies for the atrophic form of AMD or preventative strategies for inhibiting the progression from early- to late-stage AMD. The use of lasers has been considered as a possible intervention to slow progression of early-stage disease. Thermal laser photocoagulation with continuous-wave (CW) lasers was used in the 1990s and it was reported to reduce drusen load, a risk factor for progression to late-stage AMD.[10–14] However, these lasers result in thermal damage to the photoreceptors and inner retinal neurons, as the laser energy is converted to heat energy through absorption by the melanin in the RPE monolayer and choroid.[15,16] Some reports have also highlighted a potential increased risk of CNV,

subretinal fibrosis, and microscotomas.[17–20] A Cochrane review of the literature for thermal laser treatments for AMD suggests that the frequency of CNV in AMD eyes is not different between laser-treated and the natural history cohorts when laser energy is within the clinical range.[10] However, when used at high-energy levels in mice, the thermal laser burn can break Bruch's membrane, leading to the growth of new choroidal vessels into the subretinal space, mimicking the neovascular form of human AMD.[21] Because of this, photocoagulation lasers are being used at high energy to induce a model of CNV in various animals,[21] and further use of thermal lasers for prophylactic treatment for early stages of AMD has not been continued.

Ongoing studies, however, have continued with the aim to develop lasers that could induce the positive effect of drusen reduction, but without the thermal damage seen with traditional lasers. One strategy being adopted is to shorten the pulse of the laser and deliver a subvisible threshold laser spot. The 3-ns pulsed laser has similar features to conventional 532-nm CW photocoagulation lasers, but the pulse duration selectively modulates pigmented tissues while minimizing thermal damage to the delicate apposing retinal neurons.[22,23] Previously, the acute effects of the nanosecond pulsed laser have been investigated on human RPE/choroidal explants[24] and in in vivo rat models[22,23,25–27] at an energy setting similar to that used in the clinical trials. The results of these studies show that the nanosecond pulsed laser induced significantly less collateral damage than the CW laser. Recently, a pilot study has shown that low-energy, clinically appropriate nanosecond pulsed laser treatment may be useful for reducing drusen load in patients with AMD.[28–30] In mice, a clinically equivalent nanosecond laser treatment has been found to induce thinning of Bruch's membrane, which is thickened in early AMD, by modulating RPE gene expression, while producing no photoreceptor death.[29] While such short-pulse, subthreshold, low-energy treatments may eventually prove advantageous in treating AMD, the safety and specific effects of nanosecond laser treatment on retinal, RPE, and choroidal tissues requires further investigation. The aim of this study was to investigate the focal effect of nanosecond pulsed laser treatment on retinal sensitivity in humans and to detail the effects of the laser on retina, RPE, Bruch's membrane, and the vascular response in mice.

Materials and Methods

Human AMD Patients and Microperimetry Assessment

Studies involving human patients were conducted in adherence with the Declaration of Helsinki and approved by the Human Ethics Committee of the Royal Victorian Eye and Ear Hospital. A small subset of patients from pilot clinical studies investigating the efficacy of the nanosecond laser treatment in the early stages of AMD were recruited (Australian New Zealand Clinical Trials Registry; ID: ACTRN12609001056280). Participants (50–75 years) had bilateral intermediate AMD (drusen $>$ 125 μm) and best corrected visual acuity of 6/19 meters (20/63 feet) or better at baseline examination. The worst performing eye was treated with a nanosecond, ultra-low energy laser (3-ns, 2RT laser; Ellex, Adelaide, Australia) and 12 laser spots were placed just inside the superior and inferior macular arcades, with energy levels of a spot individually titrated (range, 0.15–0.45 mJ; average energy, 0.24 mJ). The 3-ns pulsed laser is a neodymium:yttrium-aluminium-garnet (Nd:YAG) laser with a wavelength of 532 nm and a fixed 400-μm-diameter spot size. The energy dose of laser administered does not cause a visible retinal effect upon treatment and has been shown to selectively ablate the RPE cells while not damaging the adjacent retinal neurons.[29] Thus, the term "subthreshold" is used to describe this laser dose. In the patients treated 7 years before the microperimetry ($n = 2$), only a single session of laser treatment was administered. In the patients treated 6 months before the microperimetry ($n = 5$), the participants had received 12 spots every 6 months for 3 years, with the most recent treatment being 6 months before this substudy. See Table 1 for details of patient visual acuity and time post laser treatment.

Table 1. Patient Data, Including Time Post Laser Treatment and Best Corrected Visual Acuity

Patient ID	Time Post Laser Treatment	Visual Acuity	
		Right Eye	Left Eye
BB	6 mo	6/7.5	6/5
BV	6 mo	6/7.5	6/6
GH	6 mo	6/6	6/7.5
HM	6 mo	6/5	6/6
IK	6 mo	6/6	6/5
MK	7 y	6/5	6/6
DC	7 y	6/6	6/6

At 6 months ($n = 5$) and 7 years ($n = 2$), visual sensitivity immediately under and in control areas surrounding the laser spot was assessed by using microperimetry as described previously,[31] but for this subset an additional individual grid was created to test around one particular laser spot previously identified on fundus autofluorescence (FAF) imaging as manifesting both hypo- and/or hyperfluorescence where the laser had been applied. In brief, 1% tropicamide and 2.5% phenylephrine were used to induce pupillary dilatation. A 1° diameter fixation target was used and Goldman III stimuli were presented against a background of 1.27 cd/m^2 using a 4 to 2 threshold strategy. The maximum stimulus luminance was 318 cd/m^2, creating a dynamic range of 36 dB. Stimulus duration was 200 ms. Corresponding FAF images of the entire macular field, used to correlate laser spots with microperimetry results, were collected with a Spectralis HRA+OCT device (Heidelberg Engineering, Heidelberg, Germany). An average result from six to nine microperimetry measurements directly under a laser spot (laser region) was compared with similar measures from an eccentricity controlled area, adjacent to the laser spot (control region), in the same assessment. This was deemed to be one of the best options to control for learning effects seen in microperimetry[31] and for potential changes in visual sensitivity with eccentricity or over time.

Animals

All experimental procedures using animals were performed in accordance with the ARVO Statement for the Use of Animals in Ophthalmic and Vision Research and The University of Melbourne Animal Ethics Committee (Ethics No. 1614030). C57BL6J mice were obtained from the Animal Resource Centre (ARC; Perth, WA, Australia). All mice (6–8 weeks of age) were housed at the University of Melbourne and maintained in plastic cages with ad libitum access to food and water, and were raised under an average light level of $<$40 lux on a 12 hour:12 hour light-dark cycle.

Nanosecond Pulsed Laser Application

Mice were deeply anesthetized by intraperitoneal injection of ketamine (60 mg/kg; Provet, Heatherton, VIC, Australia) and

xylazine (5 mg/kg; Troy Laboratories, Sydney, NSW, Australia), and topical anesthetic (0.5% Alcaine; Alcon Laboratories, Frenchs Forrest, NSW, Australia) was applied before the pupils were dilated with topical atropine (1% Atropine Sulphate; Alcon Laboratories) and phenylephrine (Minims phenylephrine hydrochloride 10%; Bausch & Lomb, North Ryde, NSW, Australia). Laser spots were delivered bilaterally to each mouse with a fine speckle beam profile through a slit lamp ophthalmoscope. Lubricating eye gel (GenTeal; Novartis Pharmaceuticals, North Ryde, NSW, Australia) was applied to prevent dehydration of the cornea, and a handheld fundus laser contact lens was used to focus the light beam onto the retina. For the subthreshold setting, the nanosecond pulsed laser was applied at 0.065 mJ (irradiance: 52 mJ/cm^2) across five spots, which was calculated to be similar to clinical doses used in the human eye for the intervention in early AMD.[28,29] For the assessment of a suprathreshold energy setting, a single laser spot was applied at a dose of 0.5 mJ (irradiance: 398 mJ/cm^2), which is greater than the dose previously shown to result in retinal photoreceptor death.[29]

Fundus Photography and Fluorescein Angiography

After subthreshold laser application (0.065 mJ), fundus photography and fluorescein angiography were performed at 7 and 90 days after treatment by using previously described techniques.[32] The 7-day time point was chosen, as previous work has identified that the RPE areas selectively ablated by the nanosecond laser are retiled by this time,[29] while the 90-day time point was chosen to assess for a delayed neovascular response. The cornea of mice was anesthetized with topical Alcaine (0.5%) and the pupils dilated with atropine (1%) and phenylephrine (10%). Lubricating eye gel was applied to prevent the dehydration of the cornea during imaging. The retinal fundi of mice were viewed and photographed with a Micron III fundus camera (Phoenix Research Labs, Inc., Pleasanton, CA, USA). All images were collected by using the specialty Micron III software (StreamPix; NorPix, Inc., Montreal, Quebec, Canada). Following a subcutaneous injection of 0.1 mL 0.2% fluorescein sodium solution (Fluorescite 10%; Alcon), fluorescein angiographs were viewed and captured with a green filter attached to the Micron III fundus camera at 5 minutes post injection. Images were exported as tagged image files (.tif) and fluorescence intensity was quantified by using a custom macro in ImageJ v1.47 (http://imagej.nih.gov/ij/; provided in the public domain by the National Institutes of Health, Bethesda, MD, USA). Specifically, laser spots observed on fundus images ($n = 2$/eye) and unlasered control regions ($n = 3$/eye) from the same eye were circled (100-pixel diameter) and these regions of interest (ROIs) transferred to the green channel of the fluorescein angiography. The green channel of the fluorescein image was standardized for contrast and the mean intensity of pixels within the circled regions was determined. A laser spot was deemed to have a significant change in fluorescein intensity if the mean intensity was greater than two standard deviations brighter than that observed in the control regions for that eye. Images were taken and analyzed from $n \geq 5$ eyes.

Optical Coherence Tomography Acquisition and Analysis

Retinal structure was evaluated at 7 and 90 days after low-energy laser treatment (0.065 mJ) by using spectral-domain optical coherence tomography (SD-OCT; Phoenix Research Labs) with guidance by live fundus imaging (Micron III retinal imaging microscope). Linear scans composed of an average from 50 frames were captured across the center of the laser sites and in regions away from the laser treatments. Images ($n \geq 5$ eyes) were exported as tagged image files (.tif) and retinal thickness was quantified by using custom segmentation software in ImageJ v1.47. The thickness of the neural retina, including the outer nuclear layer (ONL) and the inner and outer segments of the photoreceptors and retinal pigmented epithelium (IS/OS/RPE complex), was measured in OCT cross-sectional line scans.

Immunohistochemistry and Confocal Microscopy

For immunohistochemistry, the eyes were evaluated at 5 hours, 7 and 90 days after low-energy laser treatment (0.065 mJ). Specifically, the eyes were enucleated and the anterior segment and vitreous were removed. The posterior eyecups ($n \geq 5$ per experimental group) were fixed in 4% paraformaldehyde in 0.1 M phosphate buffer, pH 7.4 (PB) for 30 minutes and cryoprotected in graded sucrose (10%, 20%, 30%) in PB overnight.[33] For retinal wholemounts, the entire eyecup (retina/choroid/sclera) was processed for immunohistochemistry as described previously[32,34] and specifically below. For retinal sections, the eyecup was embedded in optimal cutting temperature (OCT) compound (Tissue-Tek; Sakura, Torrance, CA, USA), frozen at −20°C, and sectioned transversely at 14 μm on a Microm HM550 cryostat (Thermo Scientific, Walldorf, Germany). Retinal sections were collected onto polylysine-coated slides (Thermo Scientific, Soresby, VIC, Australia) and stored at −20°C. For labeling, frozen sections or whole mount eyecups were washed in PB and blocked with 10% normal goat serum (NGS), 1% bovine serum albumin (BSA), and 0.5% Triton X-100 in 0.1 M PB (pH 7.4) for 1 hour. The samples were then incubated with primary antibodies or lectins (described below) diluted in 3% NGS, 1% BSA, and 0.5% Triton X-100 in PB overnight at room temperature (sections) or 4 days at 4 °C (whole mounts). Blood vessels were labeled by using the lectin *Bandeiraea simplicifolia* BS-I Isolectin B4-FITC conjugate (IB4, 1:75, catalogue No. L2895; Sigma-Aldrich Corp., St. Louis, MO, USA). The RPE was labeled with Alexa Fluor 633-Phalloidin, a high-affinity F-actin probe that labels RPE cell membranes (1:200, Phalloidin, Cat. No. A22284; Life Technologies, Scoresby, VIC, Australia). Microglial cells were labeled by using an antibody against ionized calcium-binding adapter molecule 1 (1:1500, rabbit anti-IbA1, immunogen, synthetic peptide corresponding to the C-terminus of human IbA1: PTGPPAKKAISELP, Cat. No. 019-19741; Wako Pure Chemical Industries, Richmond, VA, USA). After labeling, and washing with PB, sections/whole mounts were incubated with secondary antibodies as required (1:500, goat anti-rabbit IgG Alexa 568; Life Technologies Australia, VIC, Australia) and DAPI nuclei stain (1:3000; Life Technologies Australia) for 1 hour (sections) or overnight (whole mounts). The samples were washed in PB then mounted with fluorescence mounting medium (Dako, North Sydney, NSW, Australia) and covered with a glass coverslip.

Images were taken with a Zeiss confocal laser scanning microscope (Zeiss, Oberkochen, Germany) by using the ×20 air objective or ×40 oil objective as required. Whole mounts were imaged by using confocal Z-stacks (1.4-μm-section thickness) through the entire retina and RPE. Magnifications varied, with scale bars digitally added to the images by Zeiss Zen offline software. Images were adjusted when appropriate for brightness, contrast and black levels in Adobe Photoshop CSE Version 4 (Adobe System, San Jose, CA, USA). Imaris software (Bitplane, MA, USA), was used for three-dimensional rendering of RPE and vasculature to assess choroidal neovascularization.

Table 2. Oligonucleotide Primers Used in Quantitative Real-Time PCR

Genes	Primer Sequences	Accession No.	Product Size, bp
Pedf	F: 5′-TCATTCACCGGGCTCTCTAC-3′ R: 5′-GCCTGCACCCAGTTGTTAAT-3′	NM_011340.3	250
Vegfa120	F: 5′-ATCTTCAAGCCGTCCTGTGTGC-3′ R: 5′-TTGGCTTGTCACATTTTTCTGG-3′	NM_001110334.1	223
Vegfa164	F: 5′-ATCTTCAAGCCGTCCTGTGTGC-3′ R: 5′-CAAGGCTCACAGTGATTTTC-3′	NM_001110333.1	224
Vegfa188	F: 5′-ATCTTCAAGCCGTCCTGTGTGC-3′ R: 5′-CACAGTGAACGCTCCAGGAT-3′	NM_031836.2	289
Hprt	F: 5′-CCTAAGATGAGCGCAAGTTGAA-3′ R: 5′-CCACAGGACTAGAACACCTGCTAA-3′	NM_013556.2	86
Gapdh	F: 5′-TGTGTCCGTCGTGGATCTGA-3′ F: 5′-TTGCTGTTGAAGTCGCAGGAG-3′	NM_008084.2	150

F, forward; R, reverse.

Transmission Electron Microscopy (TEM)

For TEM, the eyes were evaluated at 7 days after subthreshold laser treatment (0.065 mJ). Eyecups were isolated and fixed overnight in 1% paraformaldehyde, 2.5% glutaraldehyde, 3% sucrose, and 0.01% calcium chloride in PB. The eyecups were washed in cacodylate buffer, and then incubated in 0.5% OsO_4 for 1 hour. Following dehydration in methanol (70%, 80%, 90%, and 100%) and acetone (100%), eyes were embedded in an epoxy resin (ProSciTech, Queensland, Australia) and blocks were polymerized overnight at 60°C. Initially, the eyecups were sectioned at 1 μm on an ultramicrotome (Reichert-Jung Ultracut S; Reichert, Depew, NY, USA) and stained with 0.5% toluidine blue. An Axioplan microscope (Carl Zeiss, Göttingen, Germany) was used to view retinal sections for laser regions (×40 magnification under oil). To determine the ultrastructure of the RPE and Bruch's membrane in the laser regions identified, TEM was completed. The TEM method has been described previously.[29] Ultrathin sections (70 nm) were cut on the ultramicrotome, collected on copper grids, contrasted with uranyl acetate and lead citrate solutions, and viewed with a Philips CM120 electron microscope (Field Electron and Ion [FEI] Company, Hillsboro, OR, USA). The RPE and Bruch's membrane were imaged at ×2500, ×5800, and ×13500 magnification. Images were adjusted for white levels, brightness, and contrast with Adobe Photoshop CS4.

Total RNA Extraction and Quantitative Real-Time PCR

For gene expression analysis, the retina and RPE were evaluated at 3 and 7 days after suprathreshold energy laser treatment (0.5 mJ). Unlasered tissues were used as controls. Retinae were excised from the posterior eyecups, snap frozen in liquid nitrogen, and stored at −80°C until use. To isolate the RPE, the posterior eyecup was flushed with 100 μL lysis buffer (Buffer RLT, RNeasy Mini Kit; Qiagen, Valencia, CA, USA) until all RPE cells were detached from the eyecup, before being snap frozen in liquid nitrogen and stored at −80°C until use. Total RNA was isolated from frozen retinal and RPE tissue samples by using a commercially available kit (RNeasy Mini Kit for retinal tissue and RNeasy Plus Micro Kit for RPE tissue; Qiagen, Doncaster, VIC, Australia) per the manufacturer's instructions. To eliminate possible genomic DNA contamination, all samples were treated with DNase-I at room temperature for 15 minutes. The concentration and purity of RNA were detected by measuring the absorbance at 260 and 280 nm with a spectrophotometer (Nanodrop 1000; Thermo Scientific, Wilmington, DE, USA).

A qPCR angiogenesis pathway array was used to assess global changes in retina and RPE in response to suprathreshold laser (0.5 mJ) at 3 and 7 days after treatment. Specifically, retina and RPE mRNA samples were pooled from three animals ($n = 3$ per sample) each for laser-treated C57BL6J and unlasered control to maximize the amount of RNA and to minimize bias due to biological variation. Three independent experiments were performed per laser-treated and control group ($n = 3$ samples per group). 400 ng of total RNA was reverse transcribed into complementary DNA (cDNA) by using the RT^2 First Strand cDNA Kit (Qiagen, Doncaster, VIC, Australia) according to the manufacturer's instructions (RT^2 Profiler PCR Array Handbook; Qiagen). Respective negative controls, which lacked RT enzyme, were included to control for genomic contamination. The cDNA samples were combined with RT^2 SYBR Green Mastermix (Qiagen, Doncaster, VIC, Australia) and then added across an entire Mouse Angiogenesis RT^2 Profile PCR Array (Cat No. PAMM-024Z; Qiagen) 384-well plate. This array contained 84 different genes of the angiogenesis pathway, 5 housekeeping control wells, 1 genomic DNA control well, 3 reverse transcription (RT) control wells, and 3 positive PCR control wells. The cDNA was amplified by using the Applied Biosystems 7900HT Fast Real-Time PCR System (Life Technologies, Mulgrave, VIC, Australia) at 95°C for 10 minutes, followed by 95°C for 15 seconds and 40 cycles of 60°C for 1 minute. Expression data obtained with experimental groups were normalized to the average threshold cycle (Ct) value of the housekeeping genes and expressed with respect to the control group. The resultant ΔCt values were combined to calculate the average fold regulation values. Genes that were significantly different with a minimum change in expression level of 1.5-fold for experimental group versus the control were determined by a Student's *t*-test ($P < 0.05$) comparing the ΔCt values for the triplicate trials for each test sample with the ΔCt values for the control.

Standard qPCR was used to analyze specific angiogenic gene expression changes in separate retina and RPE samples at 7 days post suprathreshold laser treatment (0.5 mJ). For standard qPCR, RT reactions were performed on 150 ng (RPE samples, $n \geq 8$/treatment) and 400 ng (retinal samples, $n \geq 9$/treatment) total RNA by using random hexamer primers (Tetro; Bioline, London, UK) and subsequently diluted to 5 ng/μL. Gene expression of three *Vegfa* isoforms (*Vegf120*, *Vegf164*, and *Vegf188*) and pigment epithelium–derived factor (*Pedf*) was assessed relative to the housekeeping genes hypoxanthine guanine phosphoribosyl transferase (*Hprt*) and glyceraldehyde-3-phosphate dehydrogenase (*Gapdh*; see Table 2 for primer sequences). External standards were used to quantify gene expression. Production of the standards required sequence-

specific primers incorporating a T7-promotor sequence at the 5′ end of each forward primer and polyT15 at the 5′ end of each reverse primer. The amplified standards were transcribed into copy RNA (Megascript T7 High Yield Transcription kit; Ambion, Inc., Austin, TX, USA) and dilutions combined with yeast t-RNA (150 ng or 400 ng; Invitrogen, Carlsbad, CA, USA) to reflect the retinal total RNA amount (150 or 400 ng) used in the RT reaction. The RNA standards were reverse transcribed with the RNA samples to standardize RT efficiency.

Standard qPCR was performed on the Rotorgene V3000 (Corbett Research, Chadstone Centre, VIC, Australia) at 95°C for 3 minutes, followed by 40 cycles of 95°C for 15 seconds and 60°C for 1 minute, using a commercial reaction mixture incorporating SYBR green (SensiFast; Bioline). Respective four-point standard curves were included in every run, and standards and samples were amplified in triplicate to minimize handling error. Each primer set yielded only one product of the correct size, and negative controls were included in every run. Absolute gene copy number was calculated with reference to the standard curve (Rotorgene V6.1 software; Corbett Research) and expressed relative to *Hprt* and *Gapdh* copy number.

Statistical Analysis

All data are expressed as the mean ± standard error of the mean (SEM). Statistical significance between experimental groups were determined by 1- or 2-way analysis of variance (ANOVA) followed by a Tukey's post hoc test for multiple comparisons as required. Significance between the mean variables of two groups was performed by a Student's *t*-test. Compilation and manipulation of all data were performed on an Excel spreadsheet (Microsoft, Redmond, WA, USA). Statistical analysis was performed by using the software GraphPad Prism 6 for Windows (GraphPad Software, San Diego, CA, USA). P values less than 0.05 were considered significant and classified by asterisks: $^{*}P < 0.05$, $^{**}P < 0.01$.

Results

In Human AMD Participants, Local Retinal Sensitivity Is Not Altered by Subthreshold, Nanosecond Pulsed Laser Treatment

A small subset of AMD patients from a larger clinical trial administered subthreshold (no retinal effect), nanosecond pulsed laser treatment were followed up at 6 months ($n = 5$) and 7 years ($n = 2$), to determine if retinal sensitivity was affected by laser treatment. Retinal sensitivity was assessed directly under and surrounding the treatment spots by using microperimetry. Figures 1A through 1D show the fundus image data for a patient, 6 months after the last laser treatment. A full-color fundus image of the laser-treated eye is shown in Figure 1A, and the inset of the laser region (black square) is magnified and shown in Figure 1B. On FAF imaging, laser spots were hyper- and hypofluorescent (Fig. 1C) and the areas targeted for microperimetry analysis in the laser region (yellow circle) and the control region (light blue circle) are indicated. Figure 1D shows the corresponding microperimetry assessment. Retinal sensitivity was similar in the laser region (yellow circle) and adjacent control regions (light blue circle). Figures 1E through 1H show a participant's fundus images and sensitivity, 7 years after laser treatment. The color fundus image of the laser-treated eye is shown in Figure 1E, and the inset of the laser region (black square) is magnified and shown in Figure 1F. The laser spots were hypofluorescent on FAF imaging in this patient and the laser area targeted for microperimetry is indicated by a yellow circle, while the control region is indicated by a light blue circle (Fig. 1G). Microperimetry values under the laser region were similar to those obtained from adjacent control regions (Fig. 1H). Figure 1I shows data for average microperimetry sensitivity within control regions and laser regions for $n = 7$ individual patients. The asterisks (*) have been used to indicate the patients followed up at 7 years ($n = 2$). Overall, there was no significant loss of retinal sensitivity within laser regions (25.44 ± 1.35 dB) compared with adjacent control regions (26.5 ± 0.94 dB, paired *t*-test, $P = 0.21$). These values are similar to the published values for visual sensitivity in AMD patients assessed by microperimetry (~26.5 dB).[31]

In Mice, Local Retinal Structure Is Intact Following Subthreshold, Nanosecond Pulsed Laser Treatment

To investigate the effect of a clinically relevant, subthreshold, nanosecond laser treatment (0.065 mJ) on RPE structure over time, C57BL6J mouse eyes were collected for histology at 5 hours, 7 days, and 90 days after treatment. RPE cell membranes were labelled with phalloidin and imaged in flat mount by using confocal microscopy. In control eyes, the RPE cells had a uniform, hexagonal structure (Fig. 2A). Five hours after laser, RPE cell membranes were disrupted at the laser site, suggesting specific loss of RPE cells in this region; however, RPE cells surrounding the laser sites appeared similar to control cells (Fig. 2B). At 7 and 90 days after laser treatment, the RPE had retiled across the laser site; however, RPE cells within the laser region appeared to be larger than adjacent cells or those from control eyes (Fig. 2C, 7 days; Fig. 2D, 90 days).

Conventional CW photocoagulation lasers can induce neuronal damage in the underlying neural retina as laser irradiation is converted to thermal energy at the melanosomes of the RPE and choroid. To assess changes in retinal fundus appearance and local retinal structure following subthreshold nanosecond laser treatment (0.065 mJ), C57BL6J mouse eyes were imaged with the Micron III fundus–OCT system (Fig. 3). A control, unlasered retinal fundus is shown in Figure 3A. Laser treatments appeared as discernable, blanched regions on fundus micrographs at 7 days (Fig. 3B). This was less obvious at 90 days such that treatment spots were often difficult to determine (Fig. 3C). At both time points there were no discernable subretinal or retinal hemorrhages apparent.

Cross-sectional OCT scans were collected for analysis of retinal layer thickness and representative unlasered control eye (Fig. 3D), and laser-treated eyes at 7 days (Fig. 3E) and 90 days (Fig. 3F) are presented. Retinal layer thicknesses of control eyes (control) and laser-treated eyes, within the treated region (laser-treated) and directly adjacent to the laser-treated region within the same scan (control in scan) were assessed. There was no focal effect of nanosecond laser treatment on photoreceptor layer thickness ($n \geq 5$ per group, 2-way ANOVA, variables: time $P > 0.05$ and laser $P > 0.05$; Fig. 3G), the IS/OS/RPE complex ($n \geq 5$ per group, 2-way ANOVA, variables: time $P > 0.05$ and laser $P > 0.05$; Fig. 3H), or total retinal thickness (data not shown) at either 7 or 90 days after laser treatment.

Subthreshold Nanosecond Laser Treatment Does Not Induce Abnormal Vessel Growth

Conventional CW laser treatment has been suggested to increase CNV in AMD patients.[17–20] Commonly, this takes the form of choroidal vessels, which break through Bruch's membrane into the neural retina. To determine if subthreshold nanosecond laser (0.065 mJ) induced such effects, fluorescein angiography and correlative histology were used. In Figure 4, fundus images and corresponding fluorescein angiographs are

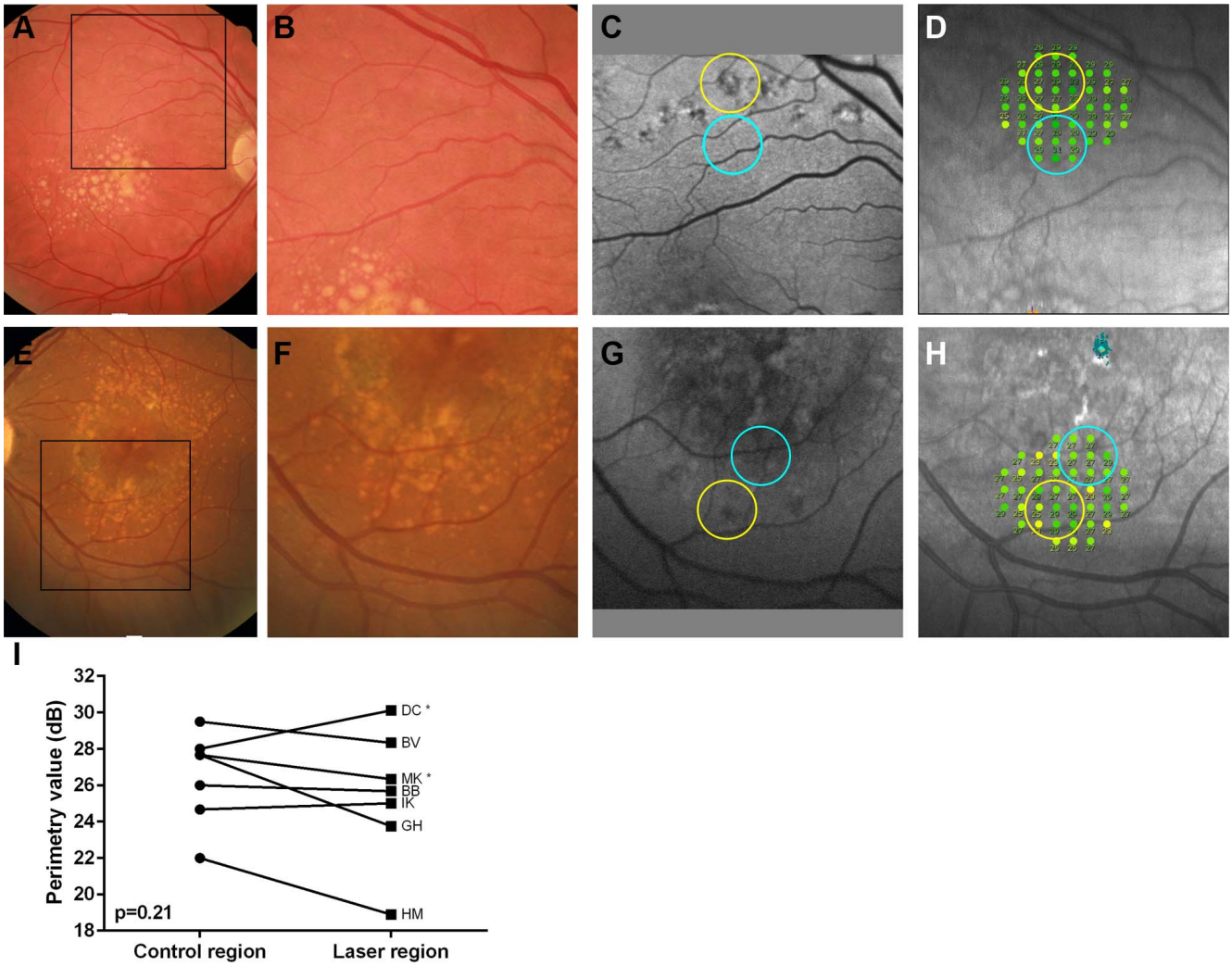

Figure 1. Microperimetry assessment of visual sensitivity in patients with AMD following nanosecond laser treatment. The effects of laser treatment on visual sensitivity directly under a laser spot were assessed with microperimetry. (**A**) The color fundus image of an AMD patient 6 months after treatment is shown, and the laser region considered for microperimetry, indicated by a *black square*, is shown magnified in (**B**). (**C**) Using FAF imaging, laser spots were evident as hyperfluorescent regions in this patient. The laser area (*yellow circle*) and the control area (*light blue circle*) targeted for microperimetry are indicated. To maintain a similar image scale and alignment between (**B–D**), some cropping of the FAF image is apparent (*gray*). (**D**) The corresponding microperimetry assessment for the patient in (**A–C**) is shown. Visual sensitivity was similar in the laser region (*yellow circle*) and adjacent control regions (*light blue circle*). (**E**) The color fundus image of an AMD patient 7 years after treatment is shown, and the laser region considered for microperimetry, indicated by a *black square*, is shown magnified in (**F**). (**G**) Using FAF imaging, laser spots were evident as hypofluorescent regions. The laser area (*yellow circle*) and the control area (*light blue circle*) targeted for microperimetry are indicated. To maintain a similar image scale and alignment between (**F–H**), some cropping of the FAF image is apparent (*gray*). (**H**) The corresponding microperimetry assessment for the patient shown in (**E–G**) is shown. Visual sensitivity was similar in the laser region (*yellow circle*) and adjacent control regions (*light blue circle*). (**I**) Graph showing average data for microperimetry sensitivity within control regions and laser regions for $n = 7$ individual patients. The $n = 2$ patients assessed at 7 years are indicated by an *asterisk*. Overall, in the short or long term, there was no significant loss of visual sensitivity within laser regions (paired *t*-test, $P = 0.21$).

presented at 7 days (Figs. 4A, 4B) and 90 days post laser (Figs. 4C, 4D). Laser regions observed on fundus images ($n = 2$/eye) and unlasered control regions ($n = 3$/eye) from the same eye were circled (Figs. 4A, 4C; example laser region indicated by black circles) and these ROIs transferred to the green channel of the fluorescein angiograph (Figs. 4B, 4D; yellow circles). The upper limit of background fluorescence for a given image was considered to be the mean intensity of the three control regions plus two standard deviations (95% confidence interval [CI]). For the purposes of graphing the laser region data, this upper limit of background fluorescence was set to 100% (Fig. 4E). A laser spot was deemed to have a significant change in fluorescein intensity if the mean intensity was greater than the upper limit of background fluorescence observed in the control regions for that eye. At 7 days, 55% (11 of 20 laser regions analyzed, $n = 5$ animals) had higher than background fluorescence (Fig. 4E). At 90 days this reduced to 20% (3 of 15 laser regions analyzed, $n = 5$ animals); however, this value is an overestimation, as laser regions were difficult to discern after 90 days and thus those that were no longer apparent could not be analyzed.

This increase in fluorescein intensity could be due to neovascularization and leaking vessels, or due to increased visibility of underlying choroidal vessels caused by melanosome reductions in laser regions. To investigate these possibilities, histology for blood vessel labeling was undertaken. Figure 5 shows transverse retinal sections taken at 7 days post laser (0.065 mJ) in control (Figs. 5A–D) and laser-treated

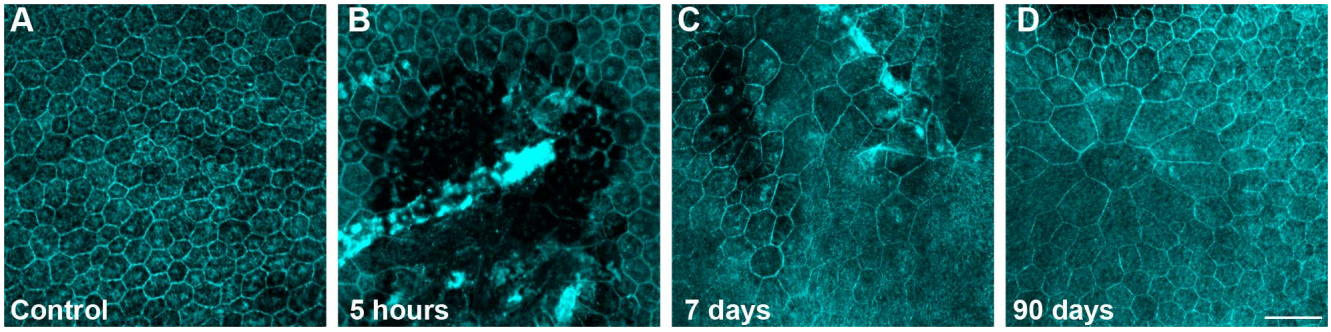

FIGURE 2. Subthreshold nanosecond laser treatment ablates RPE cells, which retile across the damaged region over time. C57BL6J mice were treated with subthreshold nanosecond laser (0.065 mJ) and the RPE was processed for histology at 5 hours, 7 days, and 3 months after treatment. (**A**) A flatmount, confocal image of a control region of RPE labeled with phalloidin shows uniform hexagonal RPE cells. (**B**) Five hours after subthreshold laser treatment the RPE membranes are disrupted and the choroidal vessels are apparent. RPE cells adjacent to the laser site are intact and appear similar to control. (**C**) Seven and (**D**) 90 days after treatment, RPE cells have spread across the laser site and consistent cell membranes are apparent. Cells appeared larger in the laser region when compared with adjacent RPE cells and those of control RPE. *Scale bar*: 50 μm.

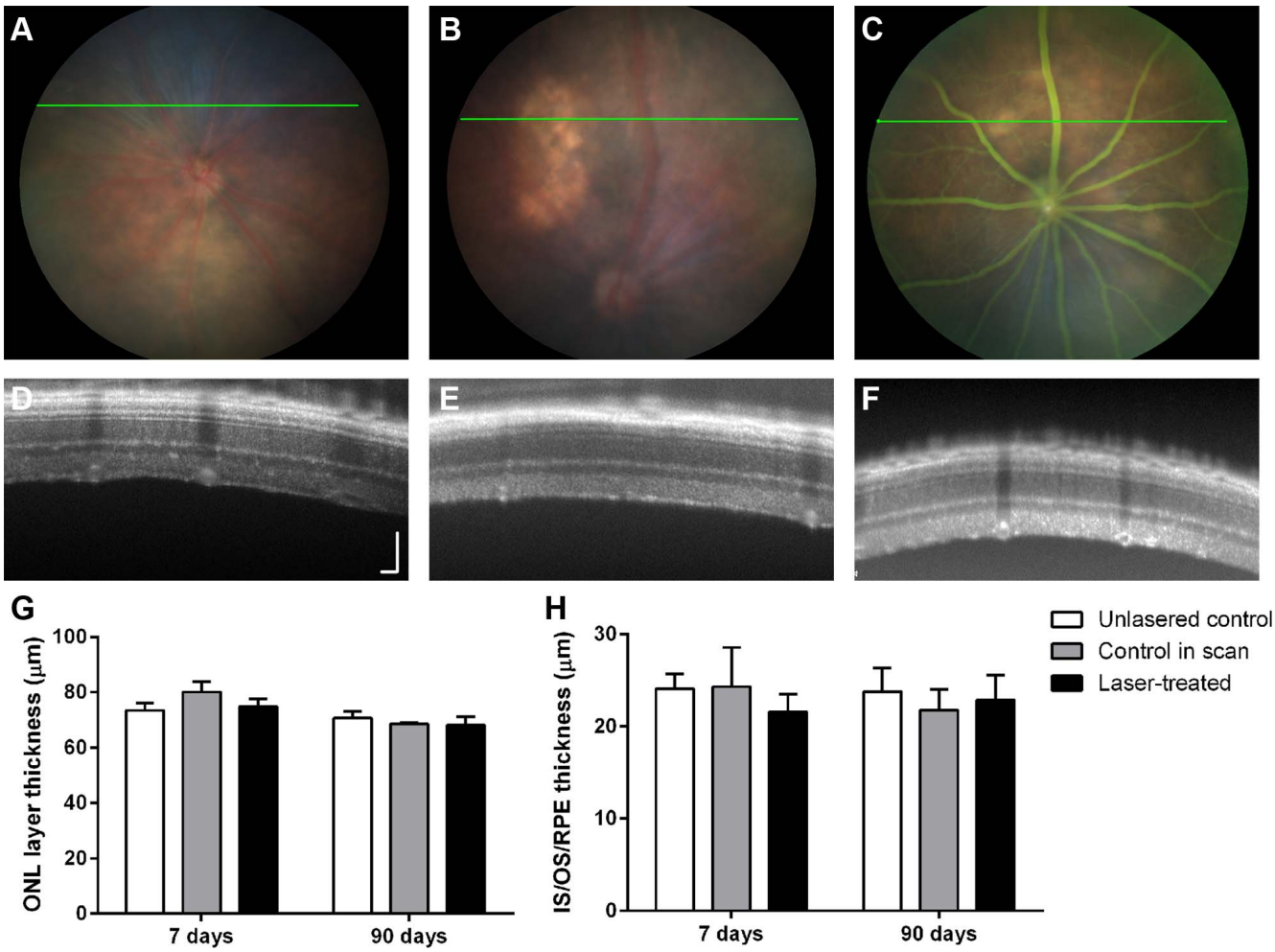

FIGURE 3. Fundus and OCT imaging of nanosecond laser treatment in mice. C57BL6J mice were treated with subthreshold nanosecond laser (0.065 mJ) and the retinal fundus was imaged with the Micron III fundus–OCT system. (**A**) A control, unlasered retinal fundus is presented. (**B**) At 7 days, laser treatments appeared as discernable, blanched regions on fundus micrographs. (**C**) At 90 days post treatment spots were often difficult to discern. There were no discernable subretinal or retinal hemorrhages apparent. (**D–F**) The corresponding cross-sectional OCT images are presented for (**D**) control, (**E**) 7 days, and (**F**) 90 days post laser. (**G**, **H**) Quantitative analysis of retinal thickness from the OCT images in control and laser regions at 7 and 90 days after laser treatment was performed. (**G**) There was no effect of laser treatment on photoreceptor layer thickness (Fig. 1G; $n > 5$ per group, 2-way ANOVA, variables: time $P > 0.05$ and laser $P > 0.05$), (**H**) or on the IS/OS/RPE complex (Fig. 1H; $n > 5$ per group, 2-way ANOVA, variables: time $P > 0.05$ and laser $P > 0.05$). Data are presented as mean ± SEM for at least $n = 5$ mice per group. *Scale* for (**D–F**): vertical, 100 μm; horizontal, 50 μm.

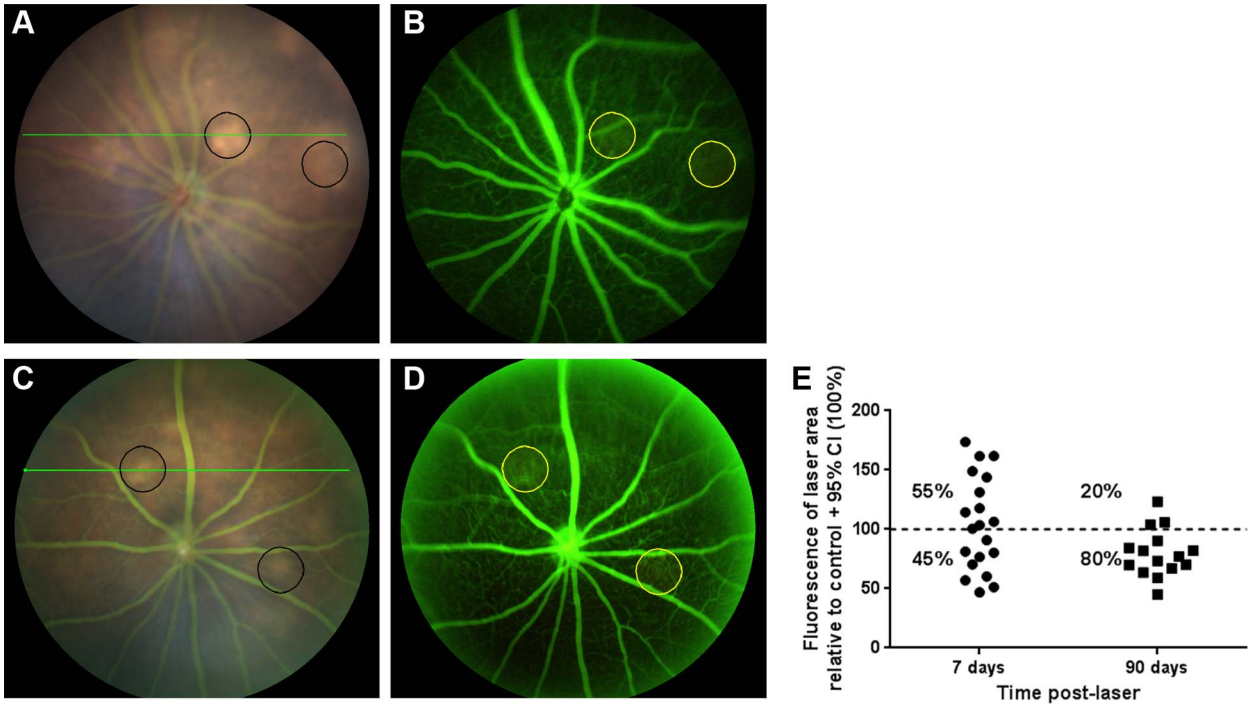

FIGURE 4. Fluorescein angiography imaging of nanosecond laser treatment in mice. C57BL6J mice were treated with subthreshold nanosecond laser (0.065 mJ) and the retinal fundus was imaged along with corresponding fluorescein angiographs with the Micron III fundus–OCT system. (**A**, **B**) At 7 days after treatment, (**A**) the fundus image shows laser treatments as blanched regions (*black circles*) and (**B**) the corresponding fluorescein angiograph shows subtle increases in fluorescein intensity associated with one of the laser sites (*upper central, yellow circle*) and less so at another site (*lower right, yellow circle*). (**C**, **D**) At 90 days after treatment, (**C**) fundus imaging shows laser treatments as subtle blanched regions (*black circles*) and (**D**) the corresponding fluorescein angiographs show either no change (*lower right, yellow circle*) or subtle increases in fluorescein intensity associated with laser site (*upper left, yellow circle*). (**E**) To determine the number of lesions with increased fluorescein leakage, pixel intensity in laser regions and control regions in the same image was analyzed. The upper limit of background fluorescence for a given image was considered to be the mean intensity of the control regions plus two standard deviations (95% CI). For the purposes of graphing the laser region data, this upper limit of background fluorescence was set to 100% (*dotted line*). A laser spot was deemed to have a significant change in fluorescein intensity if the mean intensity was greater than the upper limit of background fluorescence observed in the control regions for that eye. At 7 days, 55% of laser sites displayed an increase in fluorescein intensity. At 90 days, 20% of laser sites displayed an increase in fluorescein intensity.

regions (Figs. 5E–H), with sections imaged for brightfield, Isolectin B4–labeled blood vessels (red), IbA1-labeled microglia (green), and DAPI-labeled nuclei (blue). In control regions, Isolectin B4–labeled blood vessels (red) were apparent in the ganglion cell layer (superficial plexus), at the border of the inner nuclear and plexiform layers (intermediate plexus) and at the border of the outer nuclear and plexiform layers (deep plexus), as well as in the choroid (Ch). Microglia were closely associated with the vessels within the retina (Fig. 5B). Magnified inspection of the RPE and choroid showed intense melanin pigmentation in these tissues (Figs. 5C, 5D). Seven days post laser, treated regions of RPE showed reduced pigmentation (Fig. 5E and magnified view in Fig. 5G, yellow boxed region) and when analyzed on a scale of white (0%) to black (100%), this effect was significant (Fig. 5I; control RPE, 67% ± 1.6%, $n = 10$ control regions from $n = 5$ mice; 7-day postlaser RPE, 53% ± 0.7%, $n = 11$ laser regions from $n = 5$ animals; $^*P < 0.01$). Importantly, in these laser-treated regions the RPE remained intact and no aberrant blood vessel labeling within the photoreceptor layers, for example, was detected. Similar findings were observed at 90 days post laser (Fig. 5I).

In addition, flat-mounted retina/choroid/sclera complexes were investigated 90 days after treatment as well as three-dimensional rendering of IB4-labeled blood vessels (red) and phalloidin-labeled RPE (blue) generated from detailed confocal Z-stacks through control and laser-treated (0.065 mJ) regions. In Figure 6 fundus images, a control region (Fig. 6A, black asterisk) and laser-treated region (Fig. 6A, black circle) and the complementary fluorescein angiography (Fig. 6B; asterisk: control region, yellow circle: laser-treated region) are shown. In the control RPE region (Fig. 6C), the cells showed a uniform hexagonal structure and the choroidal vessels could not be imaged owing to strong melanosome quenching of IB4 fluorescence. In contrast, in the laser-treated region (Figs. 6D–G), changes in the RPE could be observed, including increased RPE cell size and a reduction in melanosome pigmentation, such that blood vessel labeling could be observed on the choroidal side of the laser region (Fig. 6D). However, there were no abnormal vessels observed on the photoreceptor side (Fig. 6E, rendered stack from photoreceptor nuclei to the apical RPE [blue], vessels [red]; Figs. 6F, 6G, viewed in transverse from the deep plexus to the RPE/choroid). Specifically, there was no evidence of choroidal vessels growing through the RPE into the photoreceptor layers of the retina ($n = 5$ spots/$n = 3$ animals). Together these results suggest the increase in fluorescein intensity in laser regions on fundoscopy is due to a reduction of pigmentation in the RPE, resulting in increased visibility of choroidal fluorescein labeling, and not to abnormal or leaky vessels within the retina.

Subthreshold Nanosecond Laser Treatment Does Not Disrupt the Choroidal/RPE/Photoreceptor Complex or Bruch's Membrane

To further investigate whether subthreshold nanosecond laser treatment (0.065 mJ) induced interruptions in Bruch's

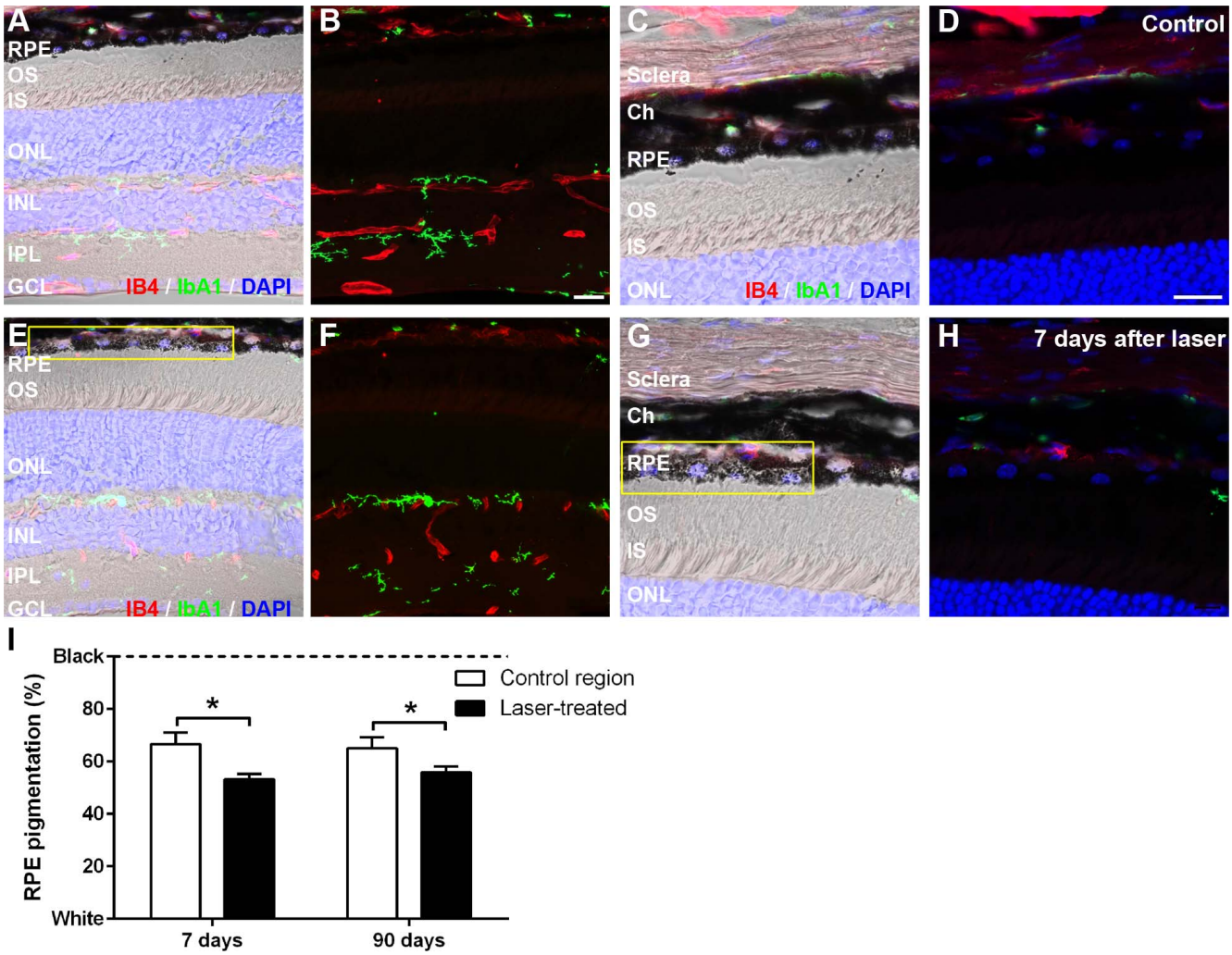

Figure 5. Histologic analysis of RPE pigment levels, blood vessels, and microglia following subthreshold nanosecond laser treatment in mice. C57BL6J mice were treated with subthreshold nanosecond laser (0.065 mJ) and 7 days later transverse retinal sections were labeled for blood vessels (IB4-lectin-647, *red*), microglia (IbA1-488, *green*), cell nuclei (DAPI, *blue*), and brightfield. (**A**, **B**) In unlasered control regions, (**A**) brightfield imaging shows the pigmented layers of the choroid and RPE. (**B**) Corresponding confocal image showing normal IB4-positive blood vessels (*red*) in the superficial, the intermediate, and the deep plexus, as well as in the choroid. IbA-1–positive microglia (*green*) were closely associated with the vessels within the retina and not present in the outer nuclear layer. (**C**, **D**) Magnified inspection of the RPE and choroid under (**C**) brightfield showed intense melanin pigmentation in these tissues and (**D**) normal vessel and macrophage labeling. (**E**–**H**) Seven days post laser, (**E**) brightfield imaging of laser-treated regions of RPE showed reduced pigmentation (*yellow boxed region*), but (**F**) normal intraretinal blood vessel and microglial morphology. (**G**, **H**) Magnified inspection of the RPE and choroid under (**G**) brightfield and (**H**) corresponding confocal imaging of vessels and macrophages, showing the RPE remains intact in laser regions (*yellow boxed region*). (**I**) Seven and 90 days post laser, images of treated regions of RPE were analyzed for pigmentary changes. On a scale of white (0%) to black (100%, *dotted line*), subthreshold laser–treated regions showed significantly less pigmentation. Data are presented as mean ± SEM for at least 10 laser regions from $n = 5$ mice per group ($^*P < 0.05$). Ch, choroid; OS, photoreceptor outer segment; IS, photoreceptor inner segment; ONL, outer nuclear layer; INL, inner nuclear layer; IPL, inner plexiform layer; GCL, ganglion cell layer. *Scale* for (**A**, **B**) and (**E**, **F**): 20 μm; (**C**, **D**) and (**G**, **H**): 20 μm.

membrane or permanent damage to the RPE, transmission electron microscopy was used. Figure 7 shows TEM of choroid, RPE, and photoreceptor outer segments (OS) in an example control (Figs. 7A–C) and laser region 7 days after treatment (Figs. 7D–F). In the control region, RPE nuclei were regularly spaced (Fig. 7A, Nu), mature melanosomes were frequent (Fig. 7B, m), and Bruch's membrane structure showed an intact five-layered structure (Fig. 7C, BM). In a region directly affected by laser treatment—although RPE nuclei were sparse, suggestive of cell loss, retiling, and spread—Bruch's membrane showed no sign of interruption (Fig. 7D). In this region, the OS appeared as small circles owing to section orientation but otherwise appeared intact. Upon magnification, the RPE in this region was found to have fewer mature melanosomes and many new melanosomes (nm) forming, at the stage III phase of melanosome development, characterized by filamentous/striated material lying within the melanosome[35,36] (Fig. 7E). Stage IV or mature melanosomes (m), characterized by a solid black appearance, were also present (Fig. 7E). In addition, detailed imaging of Bruch's membrane structure showed an intact five-layered structure across the length of the laser-treated region (Fig. 7F). These data suggest that 7 days after treatment, the nanosecond laser produced a targeted action on the RPE, without disruption of Bruch's membrane or the choroidal/RPE/photoreceptor complex even in regions directly affected by the laser.

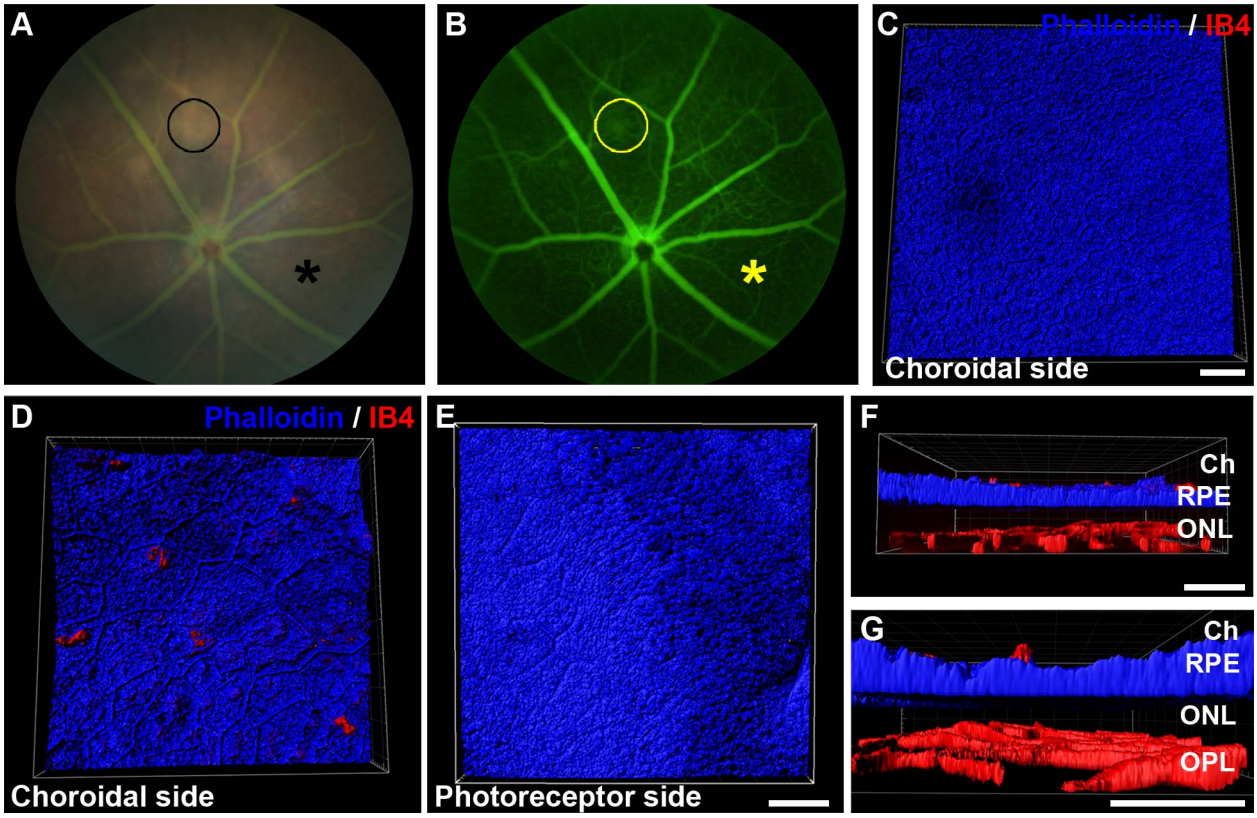

Figure 6. Whole mount confocal analysis of RPE structure and the outer retinal vasculature following subthreshold nanosecond laser treatment in mice. C57BL6J mice were treated with subthreshold nanosecond laser (0.065 mJ) and 90 days later flat-mounted retina/choroid/sclera complexes were investigated. (**A**) Fundus image and corresponding (**B**) fluorescein angiography of laser region (*yellow circle*) and control region (*asterisk*) imaged and presented in the following panels. (**C**–**G**) Three-dimensional rendered images of IB4-labeled blood vessels (*red*) and phalloidin-labeled RPE (*blue*) generated from detailed confocal Z-stacks are presented. (**C**) In the control region, the RPE cells showed a uniform hexagonal structure and the choroidal vessels could not be imaged owing to strong melanosome quenching of IB4 fluorescence. (**D**) Choroidal side view of the basal RPE in the laser region. RPE cell size increased and blood vessel labeling could be observed on the choroidal side of the laser region. (**E**) View of the RPE from the photoreceptor nuclei to the apical RPE (same area as in [**D**]), showing there are no abnormal vessels observed on the photoreceptor side of the RPE. (**F**) Side view of the RPE and vessels shown in (**D**, **E**), including rendering of the deep plexus, showing there is no abnormal vasculature in the outer nuclear layer and no choroidal neovascularization at the laser site. (**G**) Magnified view of image shown in (**F**). Ch, choroid; ONL, outer nuclear layer; OPL, outer plexiform layer. *Scale* for (**C**–**G**): 50 μm.

Nanosecond Pulsed Laser Treatment Does Not Induce Upregulation of Angiogenic Factors at Suprathreshold Doses

Day 7 post treatment is a time point during which pathologic angiogenesis is commonly reported in rodent models of photocoagulation laser-induced CNV.[21] To investigate whether nanosecond laser treatment was capable of promoting an angiogenic environment, a suprathreshold laser dose (0.5 mJ), nearly 10 times the energy of the subthreshold dose, was administered and the effects on the eye were investigated (Fig. 8). At 7 days after suprathreshold laser treatment, a distinct, white lesion could be observed on color imaging of the fundus (Fig. 8A). The area showed an annulus of fluorescein leakage around the lesion site (Fig. 8B). On OCT imaging, the retinal neuronal layers were no longer apparent in the center of the laser site and a hyperfluorescent lesion was observed. These data suggest that the suprathreshold laser dose ablates the retina and causes leakage from damaged vessels at the edge of the laser site into the retina. To assess whether new vessel growth driven by angiogenic gene changes was evident, differential expression of angiogenesis-related genes was assessed in combined retinal-RPE samples, isolated at 3 and 7 days following laser, by using an angiogenesis PCR array. The identity of mRNAs with altered expression at different time points post laser compared to untreated age-matched controls is summarized in Tables 3 and 4. Generally, angiogenic gene expression was downregulated with only 5 to 6 genes, out of 84 investigated, altered by suprathreshold nanosecond laser treatment at each time point. For example, vascular endothelial growth factor B (*Vegfb*), which is critical for stabilization of new vessels, was downregulated 1.5-fold at 7 days. The gene expression of vascular endothelial growth factor type A (*Vegfa*), the principal mediator of choroidal and retinal neovascularization development, remained unaltered at all time points examined.

To more thoroughly investigate whether angiogenesis had been induced at day 7 post suprathreshold laser treatment (0.5 mJ), the differential regulation of *VegfA* and *Pedf* was analyzed in separate RPE ($n \geq 8$) and retinal samples ($n \geq 9$; Fig. 8). The expression of three *VegfA* isoforms (*Vegf120*, *Vegf164*, and *Vegf188*) was not altered in laser-treated RPE (Fig. 8A) or retinal (Fig. 8B) samples when compared to untreated controls. Conversely, the gene expression of *Pedf*, an inhibitor of angiogenesis,[37] was found to be significantly upregulated in both RPE and retina 7 days after suprathreshold laser treatment. Together, these findings demonstrate that at suprathreshold energy settings, the nanosecond laser is unlikely to promote CNV.

Investigative Ophthalmology & Visual Science

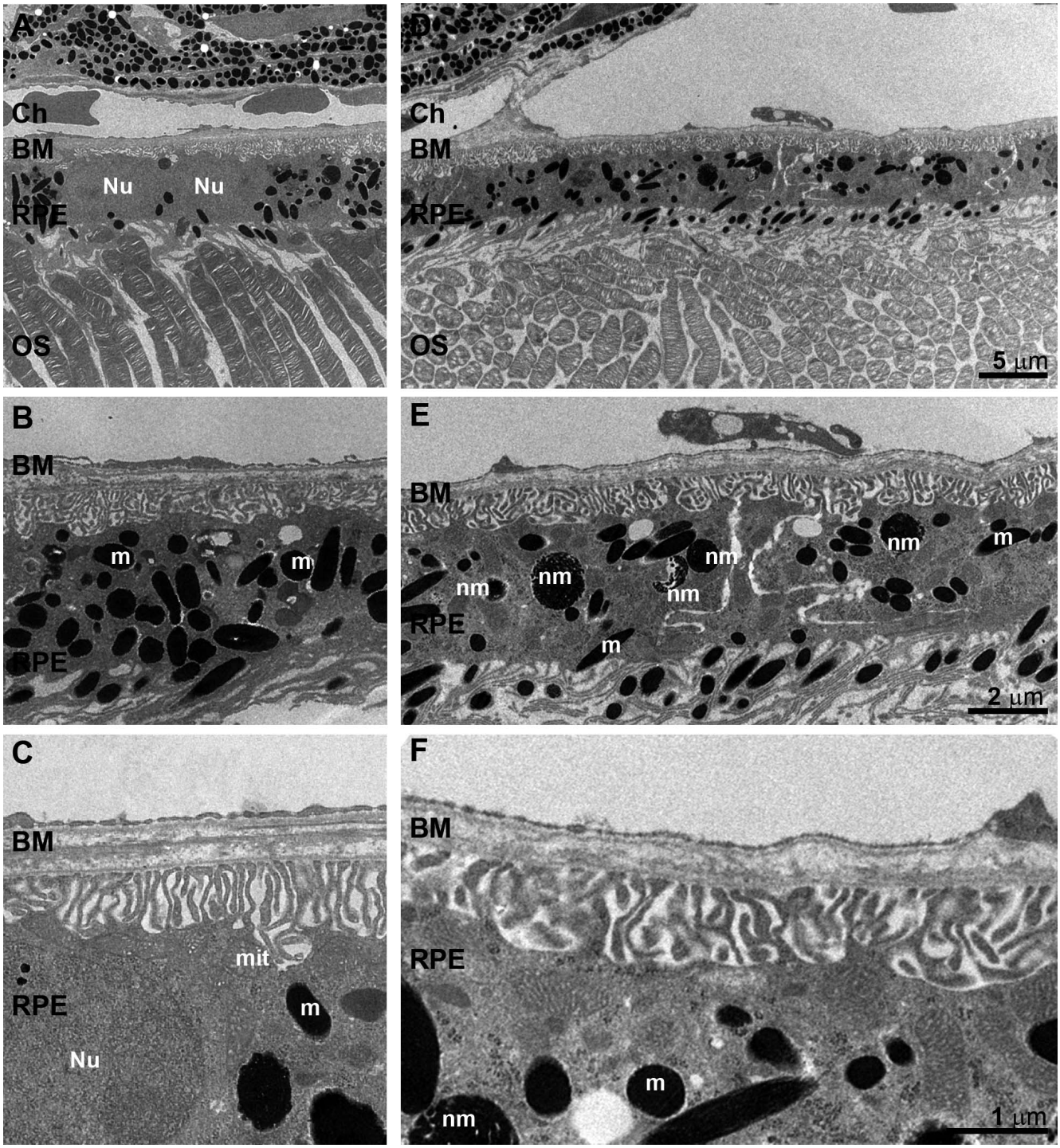

Figure 7. TEM images of RPE and Bruch's membrane (BM) structure following subthreshold nanosecond laser treatment in mice. C57BL6J mice were treated with subthreshold nanosecond laser (0.065 mJ) and 7 days later eyes were processed for TEM. (**A**, **C**) In the control region, (**A**) RPE nuclei (Nu) were regularly spaced, (**B**) mature melanosomes (m) were plentiful, and (**C**) BM showed an intact five-layered structure. (**D**–**F**) In a region directly affected by laser treatment, BM showed no sign of interruption. (**D**) In this region, the photoreceptor outer segments (OS) appeared as small circles owing to section orientation, but otherwise appeared intact. (**E**) Magnified view from (**D**), showing the RPE in this region has fewer mature melanosomes (m) and many new melanosomes (nm) forming. (**F**) Magnified view from (**E**), showing BM is intact and exhibits a five-layered structure in the laser region. Ch, choroid; mit, mitochondria. *Scale* for (**A**, **D**): 5 μm; for (**B**, **E**): 2 μm; and for (**C**, **F**): 1 μm.

Discussion

This study described the local effect of nanosecond pulsed laser treatment on retinal sensitivity in humans and correlated these findings with retinal, RPE, and Bruch's membrane structure in mice. In patients with AMD, subthreshold laser treatment did not affect retinal sensitivity assessed by microperimetry, which was similar in laser and control regions. In the mouse, retinal structure was preserved directly under the laser sites up to 3 months after treatment, reinforcing the safety

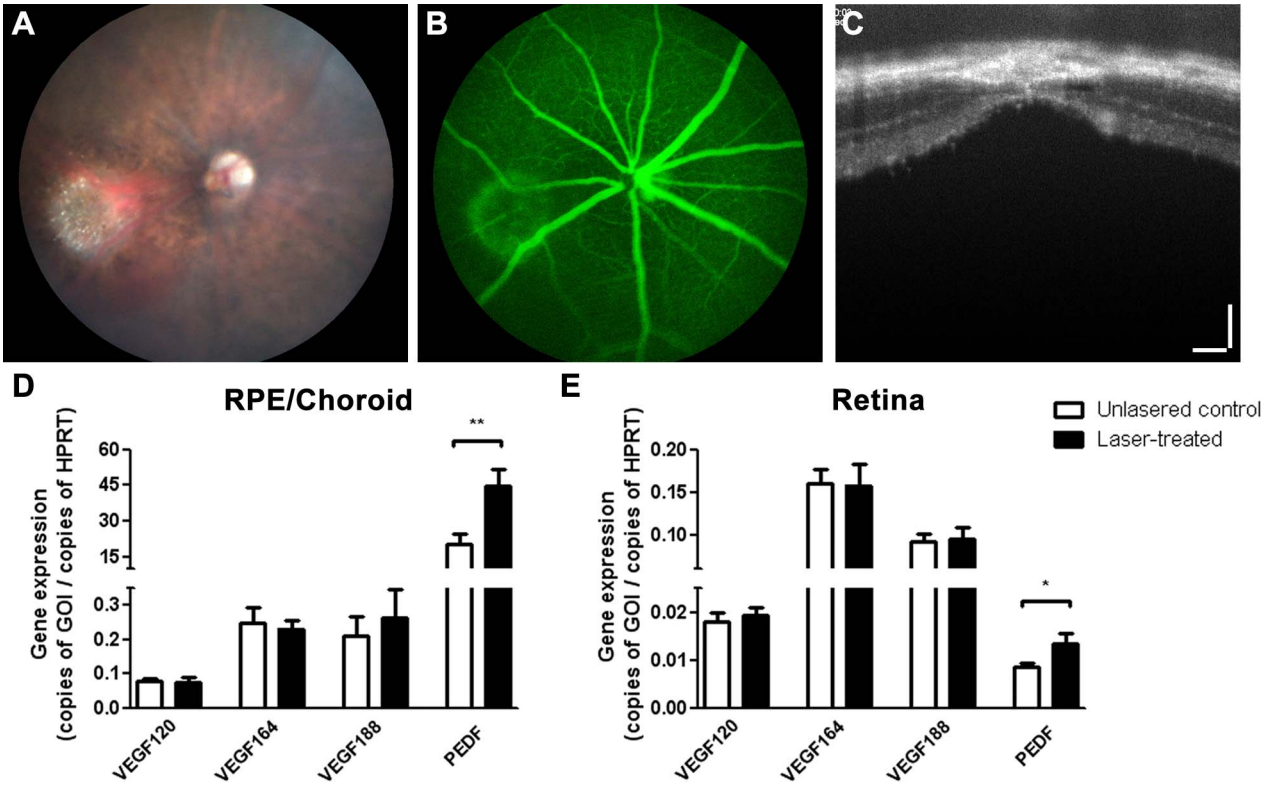

Figure 8. Suprathreshold nanosecond laser treatment causes a fundus lesion and retinal neuronal loss but little change in angiogenic gene expression in the RPE and retina in mice. C57BL6J mice were treated with suprathreshold nanosecond laser (0.5 mJ). (**A**) At 7 days, the retinal fundus was imaged with the Micron III fundus–OCT system. Color fundus imaging showed suprathreshold laser treatment induced a large white lesion. (**B**) Fluorescein angiography showed fluorescence leakage around the edges of the lesion site. (**C**) OCT imaging showed a loss of retinal neurons and a large hyperfluorescent lesion suggestive of scarring in the center of the laser site. (**D**, **E**) To determine if the suprathreshold laser dose induced gene expression changes consistent with neovascularization, the retina and RPE were isolated separately for analysis of *VegfA* isoforms (*VegfA*120, *Vegf164*, *Vegf188*) and *Pedf* relative to the housekeeping gene *Hprt*. Unlasered C57BL6J mice tissues were used as controls. (**D**) In laser-treated RPE samples, expression of *VegfA 120*, *164*, and *188* isoforms were not altered, while *Pedf* mRNA expression was upregulated when compared with unlasered controls ($^*P < 0.05$). (**E**) Similarly, in laser-treated retinal samples, expression of *VegfA 120*, *164*, and *188* isoforms were not altered, while *Pedf* mRNA expression was upregulated ($^{**}P < 0.01$). Data are presented as mean ± SEM for at least $n = 9$ mice per group. *Scale* for (**C**): vertical, 100 μm; horizontal, 100 μm.

profile of the nanosecond laser. While assessment of the RPE at the electron microscope level revealed subtle changes in melanosome composition in the laser-treated regions at 7 days, the RPE remained intact and Bruch's membrane structure was intact across the entire length of treated regions. In addition, in the mouse there were no histologic changes consistent with CNV and no evidence for angiogenic gene regulation observed with suprathreshold laser treatment. These data suggest that

Table 3. C57BL6J Mice Were Treated With Suprathreshold Nanosecond Laser (0.5 mJ) and 3 Days Later the Retina and RPE Were Combined and Isolated for PCR Array Analysis of Angiogenesis Gene Expression Relative to Unlasered C57BL6J Control Tissues

Gene Name	Gene Symbol	Fold Change	*P* Value
Upregulated genes			
Sphingosine-1-phosphate receptor 1	*S1pr1*	2.00	0.0461
Fibroblast growth factor 2	*Fgf2*	1.509	0.0235
Downregulated genes			
Matrix metalloproteinase 2	*Mmp2*	−2.031	0.0475
Colony-stimulating factor 3 (granulocyte)	*Csf3*	−1.600	0.0306
Tumor necrosis factor superfamily, member 12 (TWEAK)	*Tnfsf12*	−1.535	0.0461

Differentially expressed genes listed were considered significantly regulated when analysis showed a ≥1.5-fold change and $^*P < 0.05$.

Table 4. C57BL6J Mice Were Treated With Suprathreshold Nanosecond Laser (0.5 mJ) and 7 Days Later the Retina and RPE Were Combined and Isolated for PCR Array Analysis of Angiogenesis Gene Expression Relative to Unlasered C57BL6J Control Tissues

Gene Name	Gene Symbol	Fold Change	*P* Value
Upregulated genes			
Tissue inhibitor of metalloproteinase 1	*Timp1*	2.00	0.0142
Downregulated genes			
Plasminogen	*Plg*	−1.71	0.0145
Transforming growth factor α	*Tgfa*	−1.61	0.0151
Leukocyte cell–derived chemotaxin 1	*Lect1*	−1.59	0.0431
Vascular endothelial growth factor B	*Vegfb*	−1.53	0.0231
Endothelin 1	*Edn1*	−1.50	0.0092

Differentially expressed genes listed were considered significantly regulated when analysis showed a ≥1.5-fold change and $^*P < 0.05$.

the nanosecond laser may be advantageous for treatment of ocular disease when compared with photocoagulation lasers.

Retinal Sensitivity Is Preserved Directly Under Sites Treated With the Nanosecond Pulsed Laser in Patients With AMD

In patients with AMD, laser spots could be observed on FAF imaging as either hyper- or hypofluorescent, 6 months to 7 years after treatment. In AMD, hyperfluorescence on FAF usually indicates increases in lipofuscin/autofluorescent debris, while hypofluorescence has been attributed to RPE dropout or thinning.[38,39] The cause of these FAF changes in laser regions in patients with AMD is not clear, but laser-induced FAF changes did not correlate with a loss of visual sensitivity. Retinal sensitivity in AMD patients with drusen and pigmentary change, assessed by our group using the same microperimeter, is around 26.5 dB with a coefficient of repeatability between evaluations of between ±4.5 dB (95% CI).[31] The average microperimetry sensitivity within control regions and laser regions for the small sample of patients studied here was not different from this previously published value. In addition, there was no significant loss of retinal sensitivity within laser regions compared with adjacent control regions. While more work with a larger group of patients would be required to confirm this finding, these data suggest that even years after laser treatment (in some cases multiple treatments) and despite FAF change, local retinal sensitivity is unlikely to be adversely affected.

Neuronal Integrity Is Preserved Directly Under Sites Treated With the Nanosecond Pulsed Laser at Clinically Relevant Energy Settings in Mice

Previously, the acute effects of the nanosecond pulsed laser have been investigated in animal models, showing that the nanosecond pulsed laser induces significantly less collateral damage to neurons than CW laser treatment.[22,23,25–27,29] When used at an energy setting similar to that used in the clinical trials for AMD, nanosecond pulsed laser treatment has been found to preserve retinal integrity in humans and mice.[28–30] In the present study, using both a clinically equivalent, subthreshold laser dose (0.065 mJ) and an in vivo fundus-OCT imaging method, we showed for the first time, to our knowledge, that retinal structure directly below the sites of laser treatment is normal. Specifically, at both 7 and 90 days after treatment there were no changes in outer nuclear layer thickness, the inner segment/outer segment/RPE complex, or in total retinal thickness directly under the laser treatment sites. This suggests that after 7 days, when a potential damage response from the laser would be acute, there are no changes in retinal layer thickness that might be consistent with swelling, or inflammation (increased retinal thickness) or with neuronal loss (decreased retinal thickness) in the mouse. In addition, at 90 days, there were no notable chronic effects directly under the laser-treated regions, suggesting that the treatment does not induce a delayed effect on local retinal integrity.

Effects of Nanosecond Laser Treatment on the RPE and Bruch's Membrane in Mice

The RPE is the primary cell type targeted by the nanosecond pulsed laser. Specifically, in vivo studies in mice and rats, and ex vivo studies using human RPE/choroidal explants, suggest that the laser energy is selectively absorbed by the melanin pigment within the RPE, causing localized cell loss.[23,24,29] It has been suggested that within 1 week, the otherwise nonmitotic RPE reenters the cell cycle at the edges of the laser site, dividing to create new cells. These new cells retile over the laser region, theoretically rejuvenating the RPE with new "younger" RPE cells in these areas.[23,24,29] The results of the current study are consistent with these previous findings. At 5 hours after subthreshold laser, flat mount labeling with phalloidin, a high-affinity F-actin probe that labels RPE cell membranes, showed RPE cells were ablated. At both 7 and 90 days, retiling of RPE cells over the laser site had occurred and although the RPE cells were larger than in control regions, the cell membranes appeared intact. In transverse section, regions of RPE affected by the laser had significantly less pigment but the RPE and the adjacent retinal neurons were intact as based on histologic analysis. Further investigation of the RPE in transverse section at the TEM level indicated that the RPE remained intact, providing a continuous structure between the choroidal vessels and OS. In addition, at 7 days the remaining RPE showed signs of a healing response, with the presence of an unusually high number of early-stage melanosomes.[35,36] These data suggest that the RPE is able to spread and repair after nanosecond laser treatment, maintaining a consistent barrier between the choroid and retina.

While the RPE appeared structurally intact at the histologic level, nanosecond laser treatment has been shown to induce changes in RPE gene expression that may induce the general thinning of Bruch's membrane, evident after use of this laser.[29] This effect may be one of the therapeutic mechanisms of nanosecond laser treatment, as Bruch's membrane has been found to thicken in the early stages of AMD, reducing the flow of nutrients between the choroid and photoreceptors.[4,5,28,40–42] However, given that one of the detrimental side effects of CW photocoagulation laser treatments may be damage to Bruch's membrane and secondary CNV,[17–20] we investigated Bruch's membrane directly adjacent to sites of laser treatment. In the present study, Bruch's membrane was investigated 7 days following laser treatment, at a time when photocoagulation lasers at high-energy settings have been found to induce breaks in Bruch's membrane and CNV as based on animal models of this condition.[21] TEM imaging showed Bruch's membrane was intact across the length of the laser regions investigated, displaying an uninterrupted five-layered structure delineated by and including apparently normal basement membranes of the choriocapillaris and RPE. This suggests that when applied at a clinically relevant energy, nanosecond laser treatment does not induce breaks or overt disturbances in Bruch's membrane.

The Nanosecond Laser Does Not Induce Angiogenesis in Mice Even When Applied at Suprathreshold Energy Settings

A further range of investigations were undertaken to probe the potential of nanosecond laser treatment to induce abnormal vessel growth. Fluorescein angiography showed that following subthreshold treatment (0.065 mJ) some laser sites had higher-than-background fluorescence, consistent with either enhanced visualization of the underlying choroid or increased vascular leakage. This finding is consistent with previous studies that show fundus fluorescein angiography changes following treatment with nanosecond laser therapy in other animal models.[43] Histologic analysis suggested that at the subthreshold dose (0.065 mJ) this increase in fluorescein intensity was likely due to increased visibility of underlying choroidal vessels, due to RPE depigmentation in the laser regions. No evidence of vessels breaking through from the choroid was observed. In addition, no evidence of other abnormal vessel labeling within the retina was apparent. This

finding is consistent with the work of Chidlow et al.[23] who have shown histologically that at 7 days after nanosecond pulsed laser treatment, dark-agouti rats do not have vascular leakage or abnormal choroidal vessels even when a suprathreshold, high-energy treatment is used. We extended on this initial finding, showing that not only at 7 days, but also at 3 months, there is no histologic evidence of CNV in eyes treated with a clinically relevant laser dose (0.065 mJ).

To further investigate the potential for an angiogenic response, an array of angiogenic genes was assayed in the retina and RPE at a range of times after suprathreshold (0.5 mJ) laser treatment. Seven days after this laser dose, the neural retina was disrupted. In addition, there was fluorescein leakage at the edges of the lesion site; however, it was unclear if these changes were induction of CNV. As high-energy photocoagulation laser models of CNV commonly show a peak lesion size at 7 days,[21] we expected that if present, angiogenic gene changes would occur before the peak lesion (3 days after laser) or at the peak lesion time (7 days after laser). Only five genes were differentially regulated at day 3 post laser and six genes at day 7 post laser, when compared to untreated control eyes, suggesting that the laser treatment induced minimal change to the global angiogenic response. Moreover, most genes with altered expression in response to nanosecond laser treatment are involved in other regulatory pathways; for instance, CSF-3 and FGF-2 may be protective to neuronal cells in various models of retinal cell death[44–46] and CTGF is an essential matricellular protein that promotes the wound-healing response to injury and fibrosis, instead of angiogenesis.[47] Furthermore, *Vegfa*, the major molecular driver required to stimulate CNV development,[48,49] was not altered in expression, suggesting that at suprathreshold energy doses, the nanosecond pulsed laser does not induce this angiogenic pathway. Instead, there was increased expression of a potent antiangiogenic factor, *Pedf*,[37,50] at day 7 post suprathreshold laser treatment. Overall, these findings suggest that suprathreshold energy nanosecond laser treatments, while producing retinal disruption, do not induce a proangiogenic molecular response.

Together, our findings with the nanosecond pulsed laser demonstrate the potential beneficial safety profile of this system compared to standard photocoagulation lasers for the treatment of AMD. However, it should be noted that many of our detailed histologic experiments were completed in healthy C57BL6J mice, and experiments on mouse models with features of early AMD or full studies with patients with AMD are required to confirm a full safety profile. Importantly, a recent safety profile study of nanosecond laser therapy suggests that at a 12-month follow-up, no patients of 50 treated in the preliminary study went on to develop CNV.[28] In addition, safety trials for use of nanosecond pulsed lasers for treatment of diabetic macular edema in a clinical setting do not report abnormal angiogenesis and instead suggest a potential therapeutic benefit over photocoagulation treatments.[51,52]

In conclusion, further work is required to fully elucidate the safety profile, efficacy, and mechanism of action of nanosecond laser treatment for use in patients with AMD. However, the results of the present study suggest that when used at a clinically relevant dose, the nanosecond laser system is likely to be safe for maintaining retinal sensitivity and neuronal integrity. In addition, when administered at a clinically relevant dose, nanosecond laser therapy is unlikely to break Bruch's membrane or induce pathologic angiogenesis, providing a potential advantage over photocoagulation lasers when investigating the potential benefit of this form of treatment for ocular disease.

Acknowledgments

The authors thank Lidia Trogrlic for invaluable technical support with this project.

Supported by No. LP150100482 (ARC Linkage to ELF), No. 1061418, No. 1138253 (National Health & Medical Research Council of Australia [NH & MRC] Project Grant to ELF); NH & MRC Fellowship GNT1103013 (RHG).

Disclosure: **K.A. Vessey**, None; **T. Ho**, None; **A.I. Jobling**, None; **S.A. Mills**, None; **M.X. Tran**, None; **A. Brandli**, None; **J. Lam**, None; **R.H. Guymer**, None; **E.L. Fletcher**, None

References

1. Lim LS, Mitchell P, Seddon JM, Holz FG, Wong TY. Age-related macular degeneration. *Lancet*. 2012;379:1728–1738.
2. Fritsche LG, Fariss RN, Stambolian D, Abecasis GR, Curcio CA, Swaroop A. Age-related macular degeneration: genetics and biology coming together. *Annu Rev Genomics Hum Genet*. 2014;15:151–171.
3. Hogan MJ, Alvarado J. Studies on human macula, 4: aging changes in Bruch's membrane. *Arch Ophthalmol*. 1967;77:410–420.
4. Sarks SH. Aging and degeneration in macular region—clinico-pathological study. *Brit J Ophthalmol*. 1976;60:324–341.
5. Hogan MJ. Role of the retinal pigment epithelium in macular disease. *Trans Am Acad Ophthalmol Otolaryngol*. 1972;76:64–80.
6. Pikuleva IA, Curcio CA. Cholesterol in the retina: the best is yet to come. *Prog Retin Eye Res*. 2014;41:64–89.
7. Booij JC, Baas DC, Beisekeeva J, Gorgels TGMF, Bergen AAB. The dynamic nature of Bruch's membrane. *Prog Retin Eye Res*. 2010;29:1–18.
8. Brown DM, Kaiser PK, Michels M, et al. Ranibizumab versus verteporfin for neovascular age-related macular degeneration. *New Engl J Med*. 2006;355:1432–1444.
9. Peden MC, Suner IJ, Hammer ME, Grizzard WS. Long-term outcomes in eyes receiving fixed-interval dosing of anti-vascular endothelial growth factor agents for wet age-related macular degeneration. *Ophthalmology*. 2015;122:803–808.
10. Virgili G, Michelessi M, Parodi MB, Bacherini D, Evans JR. Laser treatment of drusen to prevent progression to advanced age-related macular degeneration. *Cochrane Database Syst Rev*. 2015;10:1–63.
11. Fine SL. Argon-laser photo-coagulation for senile macular degeneration: results of a randomized clinical-trial. *Arch Ophthalmol*. 1982;100:912–918.
12. Gross-Jendroska M, Owens SL, Flaxel CJ, Guymer RH, Bird AC. Prophylactic laser treatment to fellow eyes of unilateral retinal pigment epithelial tears. *Am J Ophthalmol*. 1998;126:77–81.
13. Parodi MB, Virgili G, Evans JR. Laser treatment of drusen to prevent progression to advanced age-related macular degeneration. *Cochrane Datatbase Syst Rev*. 2009;3:1–45.
14. Talbot JF, Bird AC. Krypton laser in the management of disciform macular degeneration. *Trans Ophthalmol Soc U K*. 1980;100:423–424.
15. Dorin G. Evolution of retinal laser therapy: minimum intensity photocoagulation (MIP): can the laser heal the retina without harming it? *Semin Ophthalmol*. 2004;19:62–68.
16. Hooper CY, Guymer RH. New treatments in age-related macular degeneration. *Clin Exp Ophthalmol*. 2003;31:376–391.
17. Bressler NM, Maguire MG, Murphy PL, et al. Macular scatter ('grid') laser treatment of poorly demarcated subfoveal choroidal neovascularization in age-related macular degeneration: results of a randomized pilot trial. *Arch Ophthalmol*. 1996;114:1456–1464.

18. Morgan CM, Schatz H, Singerman LJ, Rice TA. Atrophic creep of the retinal-pigment epithelium after focal macular photocoagulation. *Ophthalmology*. 1989;96:96–103.
19. Owens SL, Bunce C, Brannon AJ, et al. Prophylactic laser treatment hastens choroidal neovascularization in unilateral age-related maculopathy: final results of the Drusen Laser Study. *Am J Ophthalmol*. 2006;141:276–281.
20. Owens SL, Guymer RH, Gross-Jendroska M, Bird AC. Fluorescein angiographic abnormalities after prophylactic macular photocoagulation for high-risk age-related maculopathy. *Am J Ophthalmol*. 1999;127:681–687.
21. Grossniklaus HE, Kang SJ, Berglin L. Animal models of choroidal and retinal neovascularization. *Prog Retin Eye Res*. 2010;29:500–519.
22. Wood JPM, Shibeeb O, Plunkett M, Casson RJ, Chidlow G. Retinal damage profiles and neuronal effects of laser treatment: comparison of a conventional photocoagulator and a novel 3-nanosecond pulse laser. *Invest Ophthalmol Vis Sci*. 2013;54:2305–2318.
23. Chidlow G, Plunkett M, Casson RJ, Wood JPM. Investigations into localized re-treatment of the retina with a 3-nanosecond laser. *Laser Surg Med*. 2016;48:602–615.
24. Zhang JJ, Sun Y, Hussain AA, Marshall J. Laser-mediated activation of human retinal pigment epithelial cells and concomitant release of matrix metalloproteinases. *Invest Ophthalmol Vis Sci*. 2012;53:2928–2937.
25. Chidlow G, Shibeeb O, Plunkett M, Casson RJ, Wood JPM. Glial cell and inflammatory responses to retinal laser treatment: comparison of a conventional photocoagulator and a novel, 3-nanosecond pulse laser. *Invest Ophthalmol Vis Sci*. 2013;54:2319–2332.
26. Shibeeb O, Wood JPM, Casson RJ, Chidlow G. Effects of a conventional photocoagulator and a 3-ns pulse laser on preconditioning responses and retinal ganglion cell survival after optic nerve crush. *Exp Eye Res*. 2014;127:77–90.
27. Wood JPM, Plunkett M, Previn V, Chidlow G, Casson RJ. Nanosecond pulse lasers for retinal applications. *Laser Surg Med*. 2011;43:499–510.
28. Guymer RH, Brassington KH, Dimitrov P, et al. Nanosecond-laser application in intermediate AMD: 12-month results of fundus appearance and macular function. *Clin Exp Ophthalmol*. 2014;42:466–479.
29. Jobling AI, Guymer RH, Vessey KA, et al. Nanosecond laser therapy reverses pathologic and molecular changes in age-related macular degeneration without retinal damage. *FASEB J*. 2015;29:696–710.
30. Lek JJ, Brassington KH, Luu CD, et al. Subthreshold nanosecond laser intervention in intermediate age-related macular degeneration (AMD): The Laser in Early Stages of Age-Related Macular Degeneration (LEAD) Study: study design and baseline characteristics. *Clin Exp Ophthalmol*. 2016;44:118–119.
31. Wu Z, Cunefare D, Chiu E, et al. Longitudinal associations between microstructural changes and microperimetry in the early stages of age-related macular degeneration. *Invest Ophthalmol Vis Sci*. 2016;57:3714–3722.
32. Vessey KA, Waugh M, Jobling AI, et al. Assessment of retinal function and morphology in aging Ccl2 knockout mice. *Invest Ophthalmol Vis Sci*. 2015;56:1238–1252.
33. Vessey KA, Greferath U, Aplin FP, et al. Adenosine triphosphate-induced photoreceptor death and retinal remodeling in rats. *J Comp Neurol*. 2014;522:2928–2950.
34. Ho T, Jobling AI, Greferath U, et al. Vesicular expression and release of ATP from dopaminergic neurons of the mouse retina and midbrain. *Front Cell Neurosci*. 2015;9:1–15.
35. Fitzpatrick TB, Becker SW, Lerner AB, Montgomery H. Tyrosinase in human skin: demonstration of its presence and of its role in human melanin formation. *Science*. 1950;112:223–225.
36. Ghadially FN. *Ultrastructural Pathology of the Cell and Matrix*. 2nd ed. London: William Clowes (Beccles) Limited; 1982:599–622.
37. Dawson DW, Volpert OV, Gillis P, et al. Pigment epithelium-derived factor: a potent inhibitor of angiogenesis. *Science*. 1999;285:245–248.
38. Toy BC, Krishnadev N, Indaram M, et al. Drusen regression is associated with local changes in fundus autofluorescence in intermediate age-related macular degeneration. *Am J Ophthalmol*. 2013;156:532–542.e1.
39. Yung M, Klufas MA, Sarraf D. Clinical applications of fundus autofluorescence in retinal disease. *Int J Retina Vitreous*. 2016;2:12.
40. Kliffen M, van der Schaft TL, Mooy CM, de Jong PT. Morphologic changes in age-related maculopathy. *Microsc Res Tech*. 1997;36:106–122.
41. Curcio CA, Millican CL. Basal linear deposit and large drusen are specific for early age-related maculopathy. *Arch Ophthalmol*. 1999;117:329–339.
42. Reale E, Groos S, Eckardt U, Eckardt C, Luciano L. New components of 'basal laminar deposits' in age-related macular degeneration. *Cells Tissues Organs*. 2009;190:170–181.
43. Roider J, Lindemann C, el-Hifnawi el S, Laqua H, Birngruber R. Therapeutic range of repetitive nanosecond laser exposures in selective RPE photocoagulation. *Graefes Arch Clin Exp Ophthalmol*. 1998;236:213–219.
44. Oishi A, Otani A, Sasahara M, et al. Granulocyte colony-stimulating factor protects retinal photoreceptor cells against light-induced damage. *Invest Ophthalmol Vis Sci*. 2008;49:5629–5635.
45. Kojima H, Otani A, Oishi A, Makiyama Y, Nakagawa S, Yoshimura N. Granulocyte colony-stimulating factor attenuates oxidative stress-induced apoptosis in vascular endothelial cells and exhibits functional and morphologic protective effect in oxygen-induced retinopathy. *Blood*. 2011;117:1091–1100.
46. Gao H, Hollyfield JG. Basic fibroblast growth factor: increased gene expression in inherited and light-induced photoreceptor degeneration. *Exp Eye Res*. 1996;62:181–189.
47. Zhang Q, Qi Y, Chen L, et al. The relationship between anti-vascular endothelial growth factor and fibrosis in proliferative retinopathy: clinical and laboratory evidence. *Brit J Ophthalmol*. 2016;100:1443–1450.
48. Senger DR, Galli SJ, Dvorak AM, Perruzzi CA, Harvey VS, Dvorak HF. Tumor-cells secrete a vascular-permeability factor that promotes accumulation of ascites-fluid. *Science*. 1983;219:983–985.
49. Ng EW, Adamis AP. Targeting angiogenesis, the underlying disorder in neovascular age-related macular degeneration. *Can J Ophthalmol*. 2005;40:352–368.
50. Mori K, Duh E, Gehlbach P, et al. Pigment epithelium-derived factor inhibits retinal and choroidal neovascularization. *J Cell Physiol*. 2001;188:253–263.
51. Casson RJ, Raymond G, Newland HS, Gilhotra JS, Gray TL. Pilot randomized trial of a nanopulse retinal laser versus conventional photocoagulation for the treatment of diabetic macular oedema. *Clin Exp Ophthalmol*. 2012;40:604–610.
52. Pelosini L, Hamilton R, Mohamed M, Hamilton AMP, Marshall J. Retina rejuvenation therapy for diabetic macular edema a pilot study. *Retina*. 2013;33:548–558.

Investigative Ophthalmology & Visual Science